nature portfolio

https://doi.org/10.1038/s41586-021-04051-8

Supplementary information

Giant modulation of optical nonlinearity by Floquet engineering

In the format provided by the authors and unedited

Supplementary Information for
Giant modulation of optical nonlinearity by Floquet engineering

Jun-Yi Shan, M. Ye, H. Chu, Sungmin Lee, Je-Geun Park, L. Balents, and D. Hsieh

Table of contents

S1. Static single ion model

The magnetic point group of $MnPS_3$ is non-centrosymmetric ($2'/m$) with symmetry generators $\langle \sigma_v, I \otimes \mathcal{T} \rangle$, or equivalently $\langle \sigma_v, C_2' \otimes \mathcal{T} \rangle$, where σ_v is the vertical mirror perpendicular to the Mn-Mn bond, I is spatial inversion, $\mathcal{T}$ is time reversal, and C_2' is two-fold rotation along the Mn-Mn bond. In this symmetry group, ten independent nonzero $\chi_{ijk}^{ED(c)}$ elements are allowed as given below:

$$\chi_{ijk}^{ED(c)} = \left(\begin{pmatrix} \chi_{xxx} & 0 & \chi_{xxz} \\ 0 & \chi_{xyy} & 0 \\ \chi_{xxz} & 0 & \chi_{xzz} \end{pmatrix} \begin{pmatrix} 0 & \chi_{yxy} & 0 \\ \chi_{yxy} & 0 & \chi_{yyz} \\ 0 & \chi_{yyz} & 0 \end{pmatrix} \begin{pmatrix} \chi_{zxx} & 0 & \chi_{zxz} \\ 0 & \chi_{zyy} & 0 \\ \chi_{zxz} & 0 & \chi_{zzz} \end{pmatrix} \right) \tag{S1}$$

We can compute these tensor elements quantum mechanically as

$$\chi_{ijk}^{ED(c)} \propto \sum_{l,n} \left\{ \frac{\langle i|r_i|n\rangle\langle n|r_j|l\rangle\langle l|r_k|i\rangle}{(E_n - E_i - 2\hbar\omega)(E_l - E_i - \hbar\omega)} + \frac{\langle i|r_j|n\rangle\langle n|r_k|l\rangle\langle l|r_i|i\rangle}{(E_l - E_i + 2\hbar\omega)(E_n - E_i + \hbar\omega)} \right.$$
$$\left. + \frac{\langle i|r_k|n\rangle\langle n|r_i|l\rangle\langle l|r_j|i\rangle}{(E_n - E_i - \hbar\omega)(E_l - E_i + \hbar\omega)} + (j \leftrightarrow k) \right\} \tag{S2}$$

where the first sum is over Mn^{2+} ions within a unit cell, $|i\rangle$ labels the system ground state, $|l\rangle$ and $|n\rangle$ are the excited states to be summed over. In the main text we determined the resonant states involved in the ED-SHG process from the optical absorption data[1], where the initial state $|i\rangle$ is a ${}^6A_{1g}(t_{2g}^3 e_g^2)$ state, the intermediate state $|m\rangle$ is a ${}^4T_{1g}(t_{2g}^4 e_g^1)$ state, and the final state $|f\rangle$ is a charge-transferred state. Taking only permutations from near resonant states, Eqn. S2 can be simplified to

$$\chi_{ijk}^{ED(c)} \propto \sum \frac{\langle i|r_i|f\rangle\langle f|r_j|m\rangle\langle m|r_k|i\rangle}{(E_f - E_i - 2\hbar\omega - i\gamma_f)(E_m - E_i - \hbar\omega)} + (j \leftrightarrow k) \qquad \text{(S3)}$$

where γ_f is a phenomenological damping rate (section S2). To compute the matrix elements in Eqn. S3, we express the zeroth-order multi-electron wavefunctions $|i_0\rangle$, $|m_0\rangle$, and $|f_0\rangle$ in the Fock space, so that the matrix elements can be calculated using the single particle orbital wavefunctions with single particle operators. Since we are using the single ion model, the basis wavefunctions are constructed according not to the crystal symmetry, but to the Mn^{2+} site symmetry for a single $MnPS_3$ layer. The symmetry generators of the site magnetic point group are C_3 and $C_2' \otimes \mathcal{T}$, where C_3 is three-fold rotation along the z axis. The crystal field environment around Mn^{2+} is trigonal, so the original t_{2g} triplet in an otherwise octahedral environment is split into an a_1 singlet and an e doublet, where the e doublet mixes with the original octahedral e_g doublet, which we characterize by a parameter γ. Below we explicitly write out the five standard normalized single particle 3*d* wavefunctions in the trigonal crystal field and the three single particle 3*p* hole wavefunctions

$$\begin{gathered} d_1^1 = \sqrt{5}(-\frac{d_{x^2}}{2} - \frac{d_{y^2}}{2} + 2d_{z^2}) \\ d_2^{\omega} = \cos\gamma\, e_1^{(1)} + \sin\gamma\, e_1^{(2)} \\ d_3^{\omega^2} = \cos\gamma\, e_2^{(1)} + \sin\gamma\, e_2^{(2)} \\ d_4^{\omega} = -\sin\gamma\, e_1^{(1)} + \cos\gamma\, e_1^{(2)} \\ d_5^{\omega^2} = -\sin\gamma\, e_2^{(1)} + \cos\gamma\, e_2^{(2)} \\ p_1^1 = \sqrt{3}p_z, p_2^{\omega} = \sqrt{\frac{3}{2}}(p_x - ip_y), p_3^{\omega^2} = \sqrt{\frac{3}{2}}(p_x + ip_y) \end{gathered} \qquad \text{(S4)}$$

where $e^{(1)} = \left\{\sqrt{\frac{15}{2}}\left(\frac{d_{x^2}}{2} + id_{xy} - \frac{d_{y^2}}{2}\right), \sqrt{\frac{15}{2}}(\frac{d_{x^2}}{2} - id_{xy} - \frac{d_{y^2}}{2})\right\}$ and $e^{(2)} = \left\{\sqrt{\frac{15}{2}}(d_{xz} - id_{yz}), \sqrt{\frac{15}{2}}(d_{xz} + id_{yz})\right\}$ are the basis wavefunctions used in constructing the mixed *d* orbitals.

The octahedral symmetry is restored when $\cos\gamma = \sqrt{\frac{2}{3}}$ and $\sin\gamma = -\sqrt{\frac{1}{3}}$, corresponding to the absence of trigonal splitting. Here the Cartesian coordinates $\{x, y, z\}$ are aligned to be

perpendicular to the Mn-Mn bond, along the Mn-Mn bond, and along the *c* axis. The superscript on the left-hand side of each equation corresponds to the eigenvalue under C_3, where ω is the complex cubic root of one. In the case of weak trigonal splitting, the states d_1^1, d_2^ω and $d_3^{\omega^2}$ are close in energy, so we still express them as the t_{2g} manifold in Fig. 1b of the main text, while the other two *d* orbitals are expressed as e_g.

Starting from zeroth-order multielectron wavefunctions constructed from the single particle basis wavefunctions defined above, we dress $|m_0\rangle$ by both the trigonal crystal field experienced by a single Mn^{2+} site H_{tri} and spin-orbit coupling H_{SOC}, and dress $|f_0\rangle$ by H_{SOC}, so the ED transitions from $|i\rangle$ to $|m\rangle$ and from $|m\rangle$ to $|f\rangle$ are allowed since the initial and final states must have the same spin but opposite parity[2]. H_{tri} breaks local inversion symmetry and hybridizes the odd-parity $|f_0\rangle$ and the even-parity $|m_0\rangle$, whereas H_{SOC} hybridizes the final state $|f_0\rangle$ which has $S = 5/2$ with a counterpart state $|f_0'\rangle$ with opposite spin on the 3*p* hole which has $S = 3/2$. For simplicity we only consider SOC within the *p* orbitals. We express the dressing Hamiltonians as

$$H_{tri} = \sum_{\varpi,\sigma} \eta_\sigma^\varpi \, p_\sigma^{\varpi\dagger} d_\sigma^\varpi + h.c.$$
$$H_{SOC} = \sum_{\sigma\neq\sigma',\alpha,\beta} \lambda_{\sigma\sigma'}^{\alpha\beta} \, p_{\sigma,\alpha}^\dagger p_{\sigma',\beta} + h.c. \quad \text{(S5)}$$

where ϖ runs through $\{1, \omega, \omega^2\}$, σ is the spin index and α, β label the orbitals. Following an analysis using the site magnetic point group, we show that $\eta_\sigma^1 = 0$, $\eta_\sigma^\omega = -\eta_\sigma^{\omega^2} = \eta \in \mathrm{Im}$, and $\lambda_{\sigma\sigma'}^{\alpha\beta} \propto \lambda \in \mathrm{Re}$. We then use the perturbation theory to derive the dressed intermediate and final states, which yields

$$|m\rangle = |m_0\rangle + \frac{H_{f_0,f_0'}^{SOC} H_{f_0',m_0}^{tri}}{(E_{m_0} - E_{f_0'})(E_{m_0} - E_{f_0})} |f_0\rangle$$
$$|f\rangle = |f_0\rangle + \frac{H_{f_0',f_0}^{SOC}}{E_{f_0} - E_{f_0'}} |f_0'\rangle \quad \text{(S6)}$$

In the single ion model the *x* and *y* axes are equivalent, but the stacking pattern of the bulk

$MnPS_3$ crystal induces anisotropy. We incorporate this into our model phenomenologically by explicitly forcing the matrix elements $\langle p|x|d\rangle$ and $\langle p|y|d\rangle$ to be unequal. This is accomplished by introducing anisotropy parameters $b_x \neq b_y$ and multiplying the $\langle p|x|d\rangle$ and $\langle p|y|d\rangle$ terms calculated from the isotropic model above by b_x and b_y respectively.

The sum in Eqn. S3 is over the two Mn^{2+} ions in a unit cell. We note that the single-ion states involved in the calculation above require a finite expectation value for the S_z quantum number, either up or down. Therefore, if the spins are disordered no ED-SHG is allowed. If the spins are ordered, then $\chi_{ijk}^{ED(c)}$ is proportional to the AFM order parameter, i.e., $\langle S_{z,1}\rangle - \langle S_{z,2}\rangle$.

Since the site symmetry we used is higher than the crystal symmetry, our single ion model only provides a subset of the tensor element values in Eqn. S1, which we list below.

$$\begin{aligned}
\chi_{xxx}^{ED(c)} &= i\big(\langle S_{z,1}\rangle - \langle S_{z,2}\rangle\big)\lambda^2\eta^{(i)}b_x^3\cos\gamma\,(\sqrt{6}\cos\gamma - 6\cos 2\gamma)/15\sqrt{10} \\
\chi_{xxz}^{ED(c)} &= i\big(\langle S_{z,1}\rangle - \langle S_{z,2}\rangle\big)\lambda^2\eta^{(i)}b_x^2\sin 2\gamma\,(3\sqrt{2}\cos\gamma - 2\sqrt{3})/30\sqrt{5} \\
\chi_{xyy}^{ED(c)} &= i\big(\langle S_{z,1}\rangle - \langle S_{z,2}\rangle\big)\lambda^2\eta^{(i)}b_x b_y^2\cos\gamma\,(6\cos 2\gamma - \sqrt{6}\cos\gamma)/15\sqrt{10} \\
\chi_{yxy}^{ED(c)} &= i\big(\langle S_{z,1}\rangle - \langle S_{z,2}\rangle\big)\lambda^2\eta^{(i)}b_x b_y^2\cos\gamma\,(6\cos 2\gamma - \sqrt{6}\cos\gamma)/15\sqrt{10} \\
\chi_{yyz}^{ED(c)} &= i\big(\langle S_{z,1}\rangle - \langle S_{z,2}\rangle\big)\lambda^2\eta^{(i)}b_y^2\sin 2\gamma\,(3\sqrt{2}\cos\gamma - 2\sqrt{3})/30\sqrt{5}
\end{aligned} \tag{S7}$$

where the energy denominators have been dropped for clarity. However, this subset suffices to explain our static RA-SHG data since the ED-SHG amplitude in P_{in}-P_{out} geometry only contains these elements as shown below

$$\begin{aligned}
P^{(c)}(2\omega) = \cos^3\theta_i\left[\chi_{xxx}^{ED(c)}\cos^3\varphi + \left(2\chi_{yxy}^{ED(c)} + \chi_{xyy}^{ED(c)}\right)\cos\phi\sin^2\varphi\right] \\
- 2\cos^2\theta_i\sin\theta_i\,(\chi_{xxz}^{ED(c)}\cos^2\varphi + \chi_{yyz}^{ED(c)}\sin^2\varphi)
\end{aligned} \tag{S8}$$

where θ_i is the angle of incidence of the SHG probe beam and φ is the azimuthal angle.

S2. Dynamical Floquet model

In treating the time-dependent problem we neglect the pulse envelope, since the characteristic time scale of the system $h/E_g \approx 1$ fs is much shorter than our typical Gaussian pulse widths. We also note that using our experimental values of $\hbar\Omega$ = 0.66 eV and $E_{\max}^{pu}$ = 10^9 V/m, the effective Rabi frequency $\hbar\Omega^R$ is 0.4 eV and the ponderomotive energy under the effective-mass approximation[3] is 0.09 eV, which is much smaller than both $\hbar\Omega$ and $\hbar\Omega^R$. Therefore, we neglect the term quadratic in E^{pu}. Moreover, we confine ourselves to the subspace spanned by $|i\rangle$ and $|f\rangle$ because 1) the coupling between them is electric dipole allowed, 2) these two states are resonant with our SHG photon energy and their modulations are readily observed as a modulation in SHG. Coupling of $|m\rangle$ to higher energy states is possible, but the effects are negligible since their energy difference is more off resonant from the drive. Also, we find that even if the $|m\rangle$ state is hypothetically shifted down by an amount $\Delta E_{max} \approx 100$ meV as is the case for $|i\rangle$, it would only slightly change the maximum $\Delta I^{mag}/I^{mag}$ from –91 % to –88 %.

We note that in order for our analysis using $|i\rangle$ and $|f\rangle$ as pure states to be valid (main text Eqn. 3), the lifetime of these states must be sufficiently long. Otherwise, one must use density matrices to express the states, and our analysis would be invalid. It has been shown that[4] in the limit that $\gamma_f \ll \Omega^R$, where Ω^R is the Rabi frequency, the off-diagonal elements in the density matrices can be neglected and analysis using pure states is valid. In our case, γ_f is around 30 meV and Ω^R is an order of magnitude larger, so the Floquet picture is valid. We do not consider the intermediate state lifetime because it is not a relevant state in this Floquet problem.

Starting from the time-dependent Hamiltonian $H(t) = H_0 + e\vec{r}\cdot\vec{E}^{pu}\cos\Omega t$, the infinite dimensional Floquet Hamiltonian $(H_F)_{mn} = \frac{1}{2\pi/\Omega}\int_0^{2\pi/\Omega} e^{i\Omega t(m-n)}H(t) - n\hbar\Omega\delta_{mn}$ can be expressed in matrix form as

$$H_F = \begin{pmatrix} \ddots & & & & \\ & H_0 - \hbar\Omega & H_1 & & \\ & H_1 & H_0 & H_1 & \\ & & H_1 & H_0 + \hbar\Omega & \\ & & & & \ddots \end{pmatrix} \quad \text{(S9)}$$

where H_0 is the static Hamiltonian $H_0 = \begin{pmatrix} E_i & 0 \\ 0 & E_f \end{pmatrix}$ and H_1 is the coupling term $H_1 = \begin{pmatrix} 0 & \hbar\Omega^R \\ \hbar\Omega^R & 0 \end{pmatrix}$. The Rabi frequency Ω^R is proportional to E^{pu}. Due to the phenomenological in-plane anisotropy introduced in section S1, there is also an in-plane anisotropy of Ω^R. In the dynamical model we use the same ratio $b_y/b_x \sim 1.5$ as fitted from the static RA patterns.

The time-dependent eigenstates of $H(t)$ can be constructed from the eigenvalues and eigenvectors of H_F, using a general solution of the form[5],

$$\begin{aligned} |\psi_n(t)\rangle &= e^{-i\varepsilon_n t/\hbar} \sum_m e^{-im\Omega t} \left|\phi_n^{(m)}\right\rangle \quad \text{(S10)} \\ &= e^{-i\varepsilon_n t/\hbar} \sum_m e^{-im\Omega t} \left(c_{n,i}^{(m)} |i + m\hbar\Omega\rangle + c_{n,f}^{(m)} |f + m\hbar\Omega\rangle\right) \end{aligned}$$

where ε_n is the n^{th} eigenvalue of H_F and $(\ldots, c_{n,i}^{(-1)}, c_{n,f}^{(-1)}, c_{n,i}^{(0)}, c_{n,f}^{(0)}, c_{n,i}^{(1)}, c_{n,f}^{(1)}, \ldots)$ is the corresponding eigenvector, where m corresponds to the order of the Floquet sector. There are two components for each Floquet sector because H_0 is two dimensional, corresponding to the unperturbed $|i\rangle$ and $|f\rangle$.

To construct $|i'\rangle$ given in Eqn. 3 of the main text, we first determine $E_{i'} = E_i - \Delta E$ from the eigenvalues of H_F. The corresponding normalized eigenvector to the eigenvalue $E_{i'}$ is dominated by the component $c_{n,i}^{(0)}$, which corresponds to the unperturbed $|i\rangle$ in the zeroth Floquet sector, and we define $c_{n,i}^{(0)}$ to be $\cos\alpha$. Other $c_{n,i}^{(2k)}$ can be nonzero, but they are negligible compared to $\cos\alpha$. All $c_{n,i}^{(2k+1)}$ components are zero. Instead, all $c_{n,f}^{(2k+1)}$ components are nonzero, and these components all correspond to the same unperturbed $|f\rangle$ electronic state. Therefore, we sum up these contributions, each of them is a real coefficient

$c_{n,f}^{(2k+1)}$ times its corresponding phase $e^{-im\Omega t}$, and we define the summation as $\sin\alpha\, e^{i\phi(t)}$. Perturbatively, $\sin\alpha$ is proportional to E^{pu} (Fig. S1). Lastly, all $c_{n,f}^{(2k)}$ components of the eigenvector are zero. Therefore, we have

$$\begin{aligned} |i'\rangle &= e^{-i(E_i-\Delta E)t/\hbar}(\cos\alpha\,|i\rangle + \sum_k e^{-i(2k+1)\Omega t}\, c_f^{(2k+1)}|f\rangle) \\ &= e^{-i(E_i-\Delta E)t/\hbar}(\cos\alpha\,|i\rangle + \sin\alpha\, e^{i\phi(t)}|f\rangle) \end{aligned} \tag{S11}$$

While the $|i\rangle$ component has an energy of $E_i - \Delta E$ and is still nearly resonant in the SHG process, the mixed-in $|f\rangle$ components have energies of $E_i - \Delta E + (2k+1)\hbar\Omega$, which are far from resonance in the SHG process. Therefore, in the dynamical SHG calculations we only keep the $\cos\alpha\,|i\rangle$ term and neglect the $\sin\alpha\, e^{i\phi(t)}|f\rangle$ term. The same holds true for the components in the driven $|f'\rangle$ state.

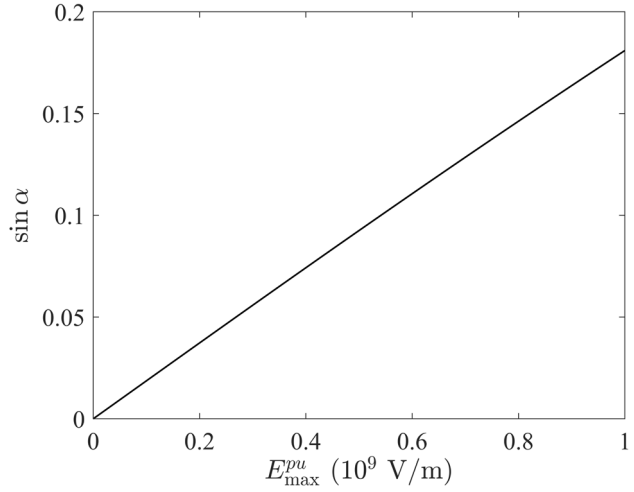

Fig. S1. The mixing factor $\sin\alpha$ as a function of $E_{\max}^{pu}$.

With the creation of Floquet sidebands as shown in Fig. 2a of the main text, an SHG spectrum would also show resonances due to these sidebands (Fig. S2). The time-averaged wavefunction amplitude of the *n*-th order sideband is approximately equal to $[\hbar\Omega^R/(E_f - E_i)]^{|n|}$. The lowest-order resonance involving the sidebands occurs at $2\hbar\omega = E_{f'} - E_{i'} \pm 2\hbar\Omega$, because the transitions involving energy $E_{f'} - E_{i'} \pm \hbar\Omega$ (e.g., from the photon-dressed states $|i' \pm \hbar\Omega\rangle$ to $|f'\rangle$) are forbidden due to parity selection rules. Since the sideband wavefunction occurs in $\chi_{ijk}^{ED(c)}$ twice (Eqn. S3), the magnitude of $\chi_{ijk}^{ED(c)}$ at the $2\hbar\omega = E_{f'} - E_{i'} \pm 2\hbar\Omega$ resonances is weaker than the main resonance at $2\hbar\omega = E_{f'} - E_{i'}$ by a factor of

$[\hbar\Omega^R/(E_f - E_i)]^4$. For $E_{\max}^{pu} = 10^9$ V/m, the resonances due to the Floquet sidebands would be weaker than the main resonance by 10^{-4}.

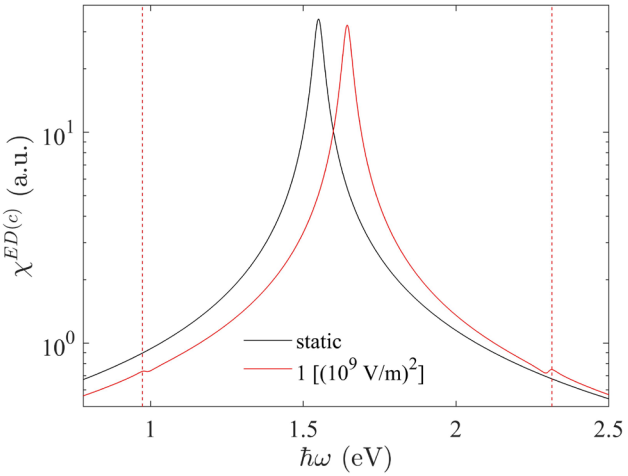

Fig. S2. The theoretical SHG spectrum within the single ion picture for both the static case and the $(E_{\max}^{pu})^2 = 1\ [(10^9\ \mathrm{V/m})^2]$ case. Resonances due to Floquet sidebands are indicated by the red dashed line. Resonances involving the $|m\rangle$ state are ignored.

For the driving frequencies in Fig. 3b of the main text, their respective $\Delta E_{\max}$ and $\sin\alpha$ with $E_{\max}^{pu} = 10^9$ V/m drive are shown in Table S1.

$\hbar\Omega$ (eV)	$\Delta E_{\max}$ (meV)	peak $\sin\alpha$ (%)
0.66	94	18.1
0.99	100	19.5
1.30	107	21.1
1.55	116	23.2

Table S1. Floquet engineering with different driving frequencies

Because these frequencies lead to similar $\Delta E_{\max}$ and $\sin\alpha$, they result in similar modulation to I^{mag}, consistent with results reported in Fig. 3b of the main text. In theory I^{mag} can be fully suppressed with larger driving amplitudes than what we used, but practically the material becomes damaged, possibly through multi-photon ionization (Keldysh parameter ~ 3 at $E_{\max}^{pu} = 10^9$ V/m).

Figures 4d and 4e of the main text show that the SHG intensity varies as a function of θ and peaks around 0° and 180°. However, there exists a small but finite offset from 0° and 180°, which is different for φ = 60° and 120°. The reason is as follows. The anisotropy in the polarization angle θ comes from two sources. The major source is the Rabi frequency anisotropy due to the layer stacking, which produces peaks at exactly 0° and 180°. The secondary source comes from the fact that the $|f\rangle$ state is not a single state but is actually a degenerate manifold of states - the excited sulfur hole and manganese electron can reside in different 3p and t_{2g} orbitals respectively (main text Fig. 1b). Upon driving, a different energy shift and mixing factor is induced between the $|i\rangle$ state and each of the different $|f\rangle$ states. Since these values all depend on the orientation of the driving field, this effect produces an additional modulation of the SHG intensity with θ. Combined with the previous source, this produces intensity peaks shifted slightly away from 0° and 180°. The coupling of the SHG probe field to each of the different $|f\rangle$ states changes depending on the polarization of the SHG probe beam φ. As a result, the θ dependence of the SHG intensity induced by the degeneracy of the $|f\rangle$ states will change depending on φ, which explains why the curves in Fig. 4d are slightly different from the curves in Fig. 4e.

S3. Calculation of photon-assisted hopping contribution

Our single ion model assumes well-localized states and neglects the band curvature. To estimate effects of band structure renormalization, we calculated the effects of photon-assisted hopping and dynamical localization within a Hubbard model[6]. In this picture the Floquet drive renormalizes the hopping parameter t to[7]

$$t_{eff} = t\sqrt{\sum_{n=-\infty}^{+\infty} \frac{J_{|n|}(\mathcal{E})^2}{1 + n\Omega/U}} \tag{S12}$$

where $J_{|n|}$ is the $|n|$-th order Bessel function, $\mathcal{E}$ is the Floquet parameter and U is the on-site Coulomb interaction parameter. Using a peak driving value of $\mathcal{E} = 0.5$, $\Omega = 0.66$ eV and $U =$ 5 eV[8], we estimate that t_{eff}/t = 1.0013. Assuming a valence bandwidth of 300 meV[9], the t amplitude modulation roughly corresponds to an energy scale of 0.4 meV, which is much smaller than the ~ 100 meV level shifts caused by the single ion effects.

References

1. Grasso, V., Neri, F., Perillo, P., Silipigni, L. & Piacentini, M. Optical-absorption spectra of crystal-field transitions in $MnPS_3$ at low temperatures. *Phys. Rev. B* **44**, 11060–11066 (1991).
2. Muthukumar, V. N., Valentí, R. & Gros, C. Microscopic model of nonreciprocal optical effects in Cr_2O_3. *Phys. Rev. Lett.* **75**, 2766–2769 (1995).
3. Kruchinin, S. Yu., Krausz, F. & Yakovlev, V. S. Colloquium: Strong-field phenomena in periodic systems. *Rev. Mod. Phys.* **90**, 021002 (2018).
4. Berman, P. R. & Malinovsky, V. S. *Principles of Laser Spectroscopy and Quantum Optics* (Princeton University Press, 2010).
5. Rudner, M. S. & Lindner, N. H. Band structure engineering and non-equilibrium dynamics in Floquet topological insulators. *Nat. Rev. Phys.* **2**, 229–244 (2020).
6. Dunlap, D. H. & Kenkre, V. M. Dynamic localization of a charged particle moving under the influence of an electric field. *Phys. Rev. B* **34**, 3625–3633 (1986).
7. Mentink, J. H., Balzer, K. & Eckstein, M. Ultrafast and reversible control of the exchange interaction in Mott insulators. *Nat. Commun.* **6**, 6708 (2015).
8. Chaudhary, S., Ron, A., Hsieh, D. & Refael, G. Controlling ligand-mediated exchange interactions in periodically driven magnetic materials. *arXiv:2009.00813 [cond-mat]* (2020).
9. Yang, J., Zhou, Y., Guo, Q., Dedkov, Y. & Voloshina, E. Electronic, magnetic and optical properties of $MnPX_3$ (X = S, Se) monolayers with and without chalcogen defects: a first-principles study. *RSC Advances* **10**, 851–864 (2020).